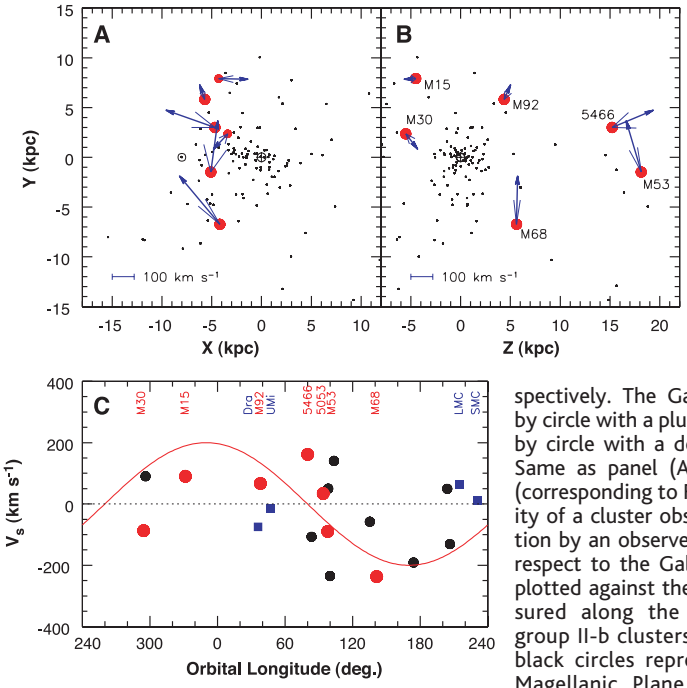

Fig. 4. Kinematic analysis for the group II-b clusters. (**A**) Space motion vectors (indicated by thick arrows) of the group II-b clusters (indicated by red circles) with the uncertainties (indicated by thin lines) (*15*) are shown in the *x*-*y* plane (corresponding to Fig. 3B). The large and small red circles represent clusters with $Z \geq 0$ and $Z < 0$ kpc, respectively. The Galactic center (indicated by circle with a plus) and the Sun (indicated by circle with a dot) are also marked. (**B**) Same as panel (A), but in the *z*-*y* plane (corresponding to Fig. 3C). (**C**) Radial velocity of a cluster observed at the Sun's position by an observer who is stationary with respect to the Galactic center (V_s) (*12*) is plotted against the orbital longitude measured along the plane defined by the group II-b clusters (*16*). Blue squares and black circles represent, respectively, the Magellanic Plane galaxies (which have their names along the edge) and globular clusters presumably associated with the Magellanic Clouds.

rograde clusters belong to the subpopulation of group I clusters having $R_G \geq 8$ kpc. Thus, it appears that, apart from a few interlopers, most clusters with $R_G \geq 8$ kpc, such as the group I clusters on retrograde orbits and our group II-b clusters, show evidence for an accreted origin from satellite systems, following the younger isochrone (Fig. 1) (*4*, *7*). We conclude that the Oosterhoff dichotomy and its close link with cluster metallicity, kinematics, and age have arisen as a result of two distinct mechanisms involved in the formation of the Galactic halo: the early formation of globular clusters in the proto-Galaxy (clusters in the inner halo and those in our group II-a) and the later accretion from satellite systems (most of the outer halo clusters, including those in our group II-b).

References and Notes

1. P. T. Oosterhoff, *Observatory* **62**, 104 (1939).
2. C. M. Clement *et al.*, *Astron. J.* **122**, 2587 (2001), and references therein.
3. H. C. Arp, *Astron. J.* **60**, 317 (1955).
4. S. van den Bergh, *Mon. Not. R. Astron. Soc.* **262**, 588 (1993).
5. There are three examples (not shown in Fig. 1) that do not fall into either of the usual Oosterhoff groups (*2*): NGC 5897 ([Fe/H] = −1.6, and $\langle P_{ab} \rangle$ = 0.83), NGC 6388 ([Fe/H] = −0.6, and $\langle P_{ab} \rangle$ = 0.71), and NGC 6441 ([Fe/H] = −0.5, and $\langle P_{ab} \rangle$ = 0.75). All these clusters have pronounced blue HB components, and their long periods may be natural consequences of the evolution from blue HB (see text). In addition, NGC 6388 and NGC 6441 show some signs of multiple stellar populations like ω Centauri; so, whether they are genuine globular clusters or not is a matter of debate (*30*).
6. Y.-W. Lee, P. Demarque, R. Zinn, *Astrophys. J.* **350**, 155 (1990).
7. S.-C. Rey, S.-J. Yoon, Y.-W. Lee, B. Chaboyer, A. Sarajedini, *Astron. J.* **122**, 3219 (2001).
8. A. Renzini, *Mem. Soc. Astron. Italiana* **54**, 335 (1983).
9. O. J. Eggen, D. Lynden-Bell, A. R. Sandage, *Astrophys. J.* **136**, 748 (1962).
10. D. A. VandenBerg, M. Bolte, P. B. Stetson, *Astron. J.* **100**, 445 (1990).
11. C. Palma, S. R. Majewski, K. V. Johnston, *Astrophys. J.* **564**, 736 (2002), and references therein.
12. R. Zinn, *Astron. Soc. Pac. Conf. Ser.* **48**, 38 (1993).
13. P. Demarque, R. Zinn, Y.-W. Lee, S. Yi, *Astron. J.* **119**, 1398 (2000).
14. R. Zinn, *Astrophys. J.* **293**, 424 (1985).
15. D. I. Dinescu, T. M. Girard, W. F. van Altena, *Astrophys. J.* **117**, 1792 (1999).
16. W. E. Kunkel, *Astrophys. J.* **228**, 718 (1979).
17. F. Fusi Pecci, M. Bellazzini, C. Cacciari, F. R. Ferraro, *Astron. J.* **110**, 1664 (1995).
18. S. van den Bergh, *Int. Astron. Union Symp.* **192**, 3 (1999).
19. D. Lynden-Bell, *Mon. Not. R. Astron. Soc.* **174**, 695 (1976).
20. W. E. Kunkel, S. Demers, *Astrophys. J.* **214**, 21 (1977).
21. R. A. Ibata, M. Irwin, G. Lewis, A. M. N. Ferguson, N. Tanvir, *Nature* **412**, 49 (2001).
22. N. B. Suntzeff, R. A. Schommer, E. W. Olszewski, A. R. Walker, *Astron. J.* **104**, 1743 (1992).
23. K. A. G. Olsen *et al.*, *Mon. Not. R. Astron. Soc.* **300**, 665 (1998).
24. J. A. Johnston, M. Bolte, P. B. Stetson, J. E. Hesser, R. S. Somerville, *Astrophys. J.* **527**, 199 (1999).
25. A. R. Walker, *Astron. J.* **104**, 1395 (1992).
26. L. T. Gardiner, T. Sawa, M. Fujimoto, *Mon. Not. R. Astron. Soc.* **266**, 567 (1994).
27. D. N. C. Lin, B. F. Jones, A. R. Klemola, *Astrophys. J.* **439**, 652 (1995).
28. D. N. C. Lin, H. B. Richer, *Astrophys. J.* **388**, L57 (1992).
29. C. Palma, W. E. Kunkel, S. R. Majewski, *Publ. Astron. Soc. Pac.* **112**, 1305 (2000).
30. C. H. Ree, S.-J. Yoon, S.-C. Rey, Y.-W. Lee, *Astron. Soc. Pac. Conf. Ser.* **265**, 101 (2002).
31. S. Yi, P. Demarque, Y.-C. Kim, *Astrophys. J.* **482**, 677 (1997).

32. Supported by the Creative Research Initiative Program of the Korean Ministry of Science and Technology.

23 April 2002; accepted 14 June 2002

A Structural Probe of the Doped Holes in Cuprate Superconductors

P. Abbamonte,[1,2*†] L. Venema,[1] A. Rusydi,[1] G. A. Sawatzky,[1‡] G. Logvenov,[3] I. Bozovic[3]

An unresolved issue concerning cuprate superconductors is whether the distribution of carriers in the CuO_2 plane is uniform or inhomogeneous. Because the carriers comprise a small fraction of the total charge density and may be rapidly fluctuating, modulations are difficult to detect directly. We demonstrate that in anomalous x-ray scattering at the oxygen K edge of the cuprates, the contribution of carriers to the scattering amplitude is selectively magnified 82 times. This enhances diffraction from the doped holes by more than 10^3, permitting direct structural analysis of the superconducting ground state. Scattering from thin films of $La_2CuO_{4+\delta}$ (superconducting transition temperature = 39 K) at temperature = 50 ± 5 kelvin on the reciprocal space intervals (0,0,0.21) → (0,0,1.21) and (0,0,0.6) → (0.3,0,0.6) shows a rounding of the carrier density near the substrate suggestive of a depletion zone or similar effect. The structure factor for off-specular scattering was less than 3×10^{-7} electrons, suggesting an absence of in-plane hole ordering in this material.

Soon after the discovery of high-temperature superconductivity, it was shown that holes doped into an antiferromagnet are unstable to the formation of charged magnetic domain lines or "stripes" with incommensurate spacing (*1*, *2*). Recent evidence from scanning tunneling microscopy (STM) suggests that the integrated local density of states at the surface of $Bi_2Sr_2CaCu_2O_{8+x}$ is indeed inhomogeneous (*3*, *4*), and when exposed to an external magnetic field spontaneously forms incommensurate "checkerboard" patterns in the vortex core (*5*). It is an issue central to research on cuprate superconductors to deter-

mine whether the local carrier density (that is, the density of doped holes) correlates spatially with these spectroscopy effects. There is therefore a tremendous need for a scattering probe of the doped holes, which could reveal their distribution in the ground state.

Incommensurate structural features have been observed in the cuprates with both x-ray and neutron diffraction (*6*). However, because the carriers comprise a very small fraction of the total charge density (about 1 part in 500 for optimally doped $La_2CuO_{4+\delta}$), x-ray scattering is normally dominated by the core electrons. Neutrons couple only to nuclei and magnetic moments and are not sensitive to charge at all. So the relationship between these observations and the distribution of carriers in the ground state, unfortunately, is unclear.

We show that, by exploiting resonance effects in the pre-edge part of the oxygen K shell of the cuprates, the amplitude for elastic x-ray scattering from doped holes can be selectively magnified by a factor of 82, enhancing diffraction from modulations in the carrier density by more than 10^3. This technique is similar to multiwavelength anomalous diffraction (*7*) or resonant magnetic x-ray scattering (*8*), in which resonance effects provide sensitivity to atomic species or the local magnetic moment, respectively. Like other scattering probes, this technique is bulk sensitive (penetration depth ~ 200 nm) and can detect fluctuating phenomena, making it kinematically complementary to STM, which detects static surface effects. The spatial resolution is modest [half-wavelength ($\lambda/2$) ~ 1.1 nm]; however, it is well-suited to mesoscopic phenomena. This is, by many standards, the first direct structural probe of the ground state in the cuprates.

We constructed a five-circle diffractometer for scattering soft x-rays. This system mimics the functionality of a single-crystal diffractometer but operates in a vacuum of 2×10^{-10} mbar (*9*). The specimens studied were thin films of oxygen-doped $La_2CuO_{4+\delta}$ grown epitaxially on $SrTiO_3$ (*10*, *11*). Samples with atomic-scale perfection were essential for cleanly demonstrating resonance effects.

The resonant enhancement is a soft x-ray spectroscopy effect that can be understood as follows. The high–superconducting transition temperature (high-T_c) materials exhibit Cu*L* (933 eV) and O*K* (534 eV) edges, which correspond to removal of an electron from Cu2*p* and O1*s* inner shells, respectively. In x-ray absorption spectra (XAS) of the insulating cuprates, the O*K* edge shows a "prepeak" feature (538 eV) that is an intersite O1*s* → Cu3*d* transition (*12*) brought about by *p-d* hybridization. The Cu*L* edge comprises two enormous peaks (Fig. 1B), which are onsite, dipole-allowed $2p \rightarrow 3d$ transitions where the hole has $j = 1/2$ or $3/2$ (*12*). Because the valence states are polarized in the CuO_2 plane, both the oxygen prepeak and the Cu*L* features are observable in XAS only when $\mathbf{E} \| ab$ (*13*).

When the system is doped, added holes go into O2*p* states (*14*); and a second prepeak, which we will refer to as the "mobile carrier peak" (MCP), appears at 535 eV (Fig. 1, red circles). Its oscillator strength builds rapidly with hole concentration as states near the Fermi level are vacated and also as spectral weight is transferred to 535 eV from the feature at 538 eV (*12*). A transfer of spectral weight with doping is the classic signature of a correlated system (*15*), and it makes the optical response at 535 eV extremely sensitive to the local hole density.

This sensitivity influences diffraction because the amplitude for light scattering from a material is proportional to the dielectric susceptibility, $\chi(\mathbf{k},\omega)$ (*16*). χ is related to XAS through the absorption coefficient $\mu = 2k\,\mathrm{Im}(n)$, where $n = \sqrt{(1+\chi)}$ (in SI units) (*17*). We can quantify the size of the resonance at the MCP by calculating $\mathrm{Im}[n(\omega)]$ from μ, Kramers-Krönig transforming to get $\mathrm{Re}[n(\omega)]$ and computing χ. Using the tabulated atomic scattering factors to set the absolute scale, we have determined χ for optimally doped $La_2CuO_{4+\delta}$ (Fig. 2).

If the carrier density is inhomogeneous, the MCP will be modulated in real space, enhancing diffraction of 535-eV x-rays. In carrier-depleted regions, the MCP will be nonexistent and χ will have its pre-resonance value. In carrier-rich regions, the peak will be enhanced. To quantify the difference, we define a contrast variable $\Delta \equiv |(\chi_{\mathrm{doped}} - \chi_{\mathrm{insulating}})/\chi_{\mathrm{insulating}}|$, which far from resonance is determined by the electron density to be ~1/500. According to Fig. 2, at the MCP Δ has the value 0.16. In other words, at 535 eV the scattering amplitude from doped holes is enhanced by $0.16 \times 500 = 82$, increasing the scattered intensity from variations in hole density by $(82)^2$ or more than 10^3.

The resonance at the Cu*L* threshold, incidentally, is truly enormous. Defining χ_{CuL} as the susceptibility at 933 eV and χ_{offres} as the value 20 eV below the edge (Fig. 2B), the quantity $|(\chi_{CuL} - \chi_{\mathrm{offres}})/\chi_{\mathrm{offres}}| \sim 0.78$. In terms of anomalous scattering factors, this gives $\Delta f \sim 136$. This feature is not strongly doping-dependent, so it does not aid our study of the carriers, but it demonstrates how large resonance effects in the soft x-ray regime can be.

The carrier enhancement can be demonstrated in the energy- and angle-dependent reflectivity of a $La_2CuO_{4+\delta}$ film (Fig. 3). In this measurement, one might expect interference fringes with angular maxima at $2d\sin(\theta) = n\lambda$. However, at $\omega = 533$ eV, labeled "a" in Fig. 1A, fringes are hardly

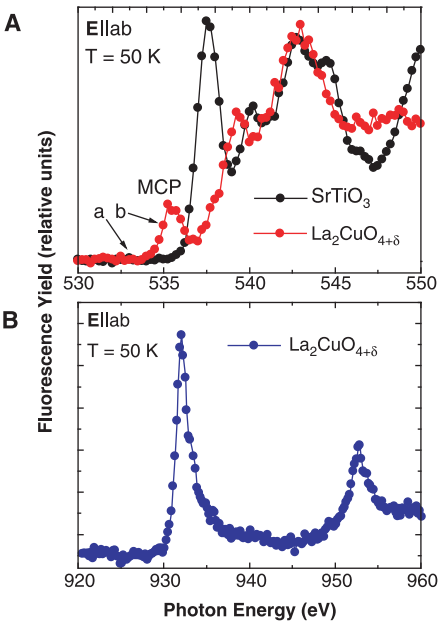

Fig. 1. X-ray absorption spectra of optimally doped $LaCuO_{4+\delta}$ and $SrTiO_3$, taken in fluorescence yield mode (**A**) in the vicinity of the O*K* edge, showing the mobile carrier peak set off from other features, and (**B**) at the Cu*L* edge. All spectra are for $\mathbf{E} \| ab$.

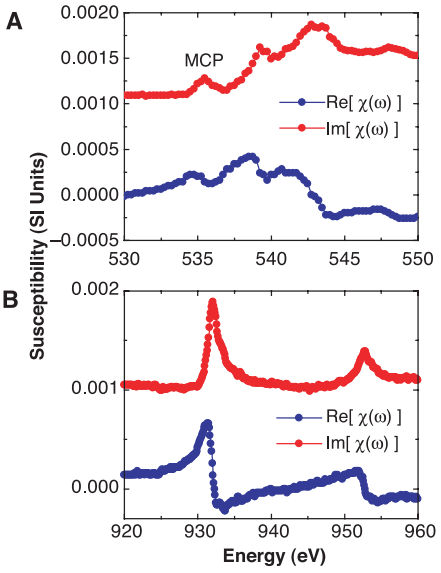

Fig. 2. *ab*-plane susceptibility of optimally doped $La_2CuO_{4+\delta}$, in SI units, calculated by the procedure described in the vicinity (**A**) of the O*K* edge and (**B**) of the $CuL_{2,3}$ edge.

[1]Materials Science Centre, University of Groningen, 9747 AG Groningen, Netherlands. [2]National Synchrotron Light Source, Brookhaven National Laboratory, Upton, NY 11973, USA. [3]Oxxel GmbH, Bremen, D-28359, Germany.

*To whom correspondence should be addressed. E-mail: peter@bigbro.biophys.cornell.edu
†Present address: Physics Department, Cornell University, Ithaca, NY 14853–2501, USA.
‡Present address: Department of Physics and Astronomy, University of British Columbia, Vancouver, BC 46T 1Z1, Canada.

visible (Fig. 3A, blue circles). This is because off resonance, the optical constants are determined by the electron density, and the density of the $SrTiO_3$ substrate (5.12 g/cm^3) and the strained film (<6 g/cm^3) do not differ significantly. So optically the film/substrate ensemble looks like a semi-infinite layer with reflectivity given by the Fresnel formulas. However, if the energy is changed by only 2 eV to the MCP (point "b" in Fig. 1A), there is a 16% boost in the film susceptibility and pronounced interference fringes appear (Fig. 3A, red circles).

The striking thing about these fringes is that they come only from the carriers and are not related to the rest of the electrons in the film. If there were carrier ordering along the (001) direction, it would be reflected as a modulation of the envelope of these fringes. Ordering parallel to the CuO_2 planes would result in scattering in an off-specular geometry; that is, in which the momentum transfer vector **q** has a component in the in-plane direction.

The enormity of the Cu*L* effects is also demonstrable in this measurement. At the top of the Cu$L_{3/2}$ peak, the interference fringes, which are barely visible off resonance, approach 10^6 photons/s (Fig. 3B, black line). Reflectivity over the full angular range for several x-ray energies is shown in Fig. 3B.

Because the prepeak and Cu*L* edge features are polarized, and we have P polarized light, one expects the interference fringes to grow toward higher scattering angles where **E** lies along the CuO_2 planes. The Cu*L* fringes at 933 eV do exactly that. The fringes at the MCP, unexpectedly, attenuate at higher angles. This can be understood in terms of a smoothing of the carrier density at the substrate. In general, what makes a layer exhibit interference fringes is two localized discontinuities (the front and rear faces) that generate waves that beat against one another as the film is rotated. The fringes will damp if one or both of these discontinuities is smeared over a depth larger than λ/2. Several things could potentially do this in our case: (i) a carrier depletion region due to the contact potential difference between the film and substrate, (ii) oxygen interdiffusion at the substrate, or (iii) structural reconstruction at the film-substrate interface induced by the polar nature of a (001) surface.

Without specifying the cause, the effect of smoothing can be demonstrated in the Born approximation, in which the scattering amplitude can be expressed in terms of one-dimensional integrals of the form

$$\chi(q) = \int_{-\infty}^{\infty} dx \chi(x) e^{iqx} \qquad (1)$$

where $\chi(x)$ is the spatially varying susceptibility and $q = 4\pi/\lambda \sin(\theta)$ is the momentum transfer. For an isotropic film of thickness L with susceptibility χ_F on a substrate with susceptibility χ_S, this integral has the value

$$\chi(q) = \frac{\chi_F}{iq}(1 + e^{-iqL}) - \frac{\chi_S}{iq + \eta} \qquad (2)$$

where a convergence factor $e^{-\eta x}$ attenuates the substrate at infinite distances. If the film is anisotropic, the susceptibility is a tensor

$$\chi(q) = \begin{pmatrix} \chi_{ab}(q) & 0 \\ 0 & \chi_c(q) \end{pmatrix} \qquad (3)$$

in which case the scattering matrix element, incorporating polarization effects, has the form

$$M = \varepsilon_1 \cdot \chi(q) \cdot \varepsilon_2 \qquad (4)$$

where ε_1 and ε_2 are the incident and scattered polarizations. Taking $\chi_S = 1$, $\chi_F{}^c = 1.03$, and $\chi_F{}^{ab} = 1.16$ at the prepeak and $\chi_F{}^{ab} = 1.78$ at the Cu$L_{3/2}$ peak, we plot $|M|^2$ in Fig. 4 for both a sharp film profile and one that has been smoothed over 20 Å at the substrate. For a sharp layer, the fringes at the carrier prepeak increase at high angles as expected. When the interface is smoothed, they fade away. So the absence of fringe enhancement at high angles is suggestive of a depletion zone or similar effect at the interface.

In an effort to corroborate the measurements of (*3*), we scanned the off-specular reciprocal space interval (0,0,0.6) → (0.3,0,0.6). The sample temperature was 50 ± 5 K, which is above T_c. The elastic scattering signal was below our fluorescence background of 1300 Hz. Using the specular measurements as a reference and scaling, this indicates a structure factor for doped holes on this interval of less than 3×10^{-7} electrons, suggesting an absence of in-plane carrier modulation in this material. Whether inhomogeneity is induced below T_c or exists in other cuprates remains to be determined.

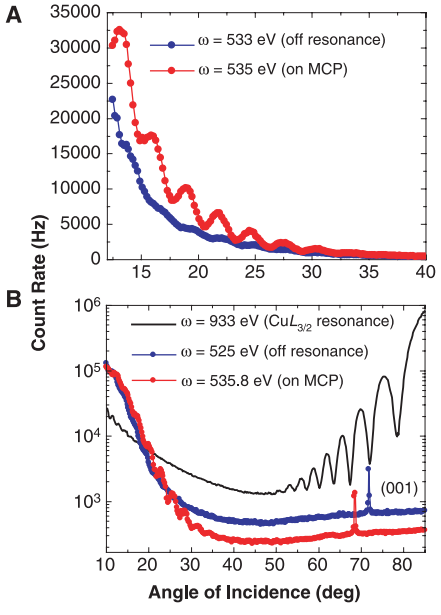

Fig. 3. Reflectivity of a 23.2-nm $La_2CuO_{4+\delta}$ film (T_c = 39 K) (**A**) just below and on the mobile carrier peak at 535 eV, showing the resonant enhancement; and (**B**) over the full angular range for three different energies. The 525-eV and 535.8-eV scans correspond to the reciprocal space interval (0,0,0.21) → (0,0,1.21), whereas the 933-eV scan corresponds to (0,0,0.37) → (0,0,2.15). The feature at 70° is the (001) Bragg reflection.

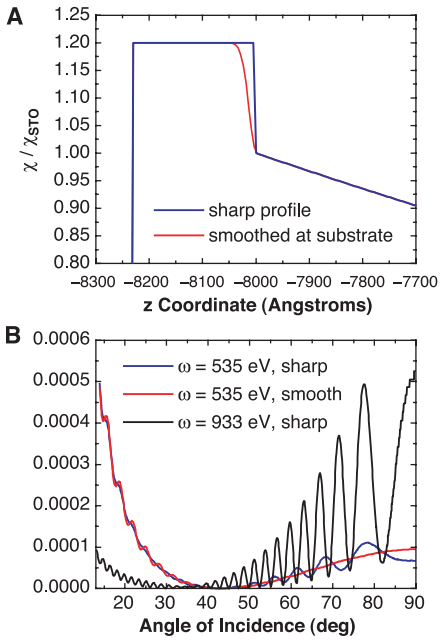

Fig. 4. (**A**) Susceptibility profiles for a perfect film on a substrate (blue line) and one that has been smoothed at the interface (red line). The sloping nature of the substrate ($x > -8000$ Å) is a numerical implementation of the factor $e^{-\eta x}$. (**B**) Interference fringes resulting from the two profiles (in relative units) showing damping at high scattering angles for the smoothed layer. Formatting is for comparison to Fig. 3B.

References and Notes

1. J. Zaanen, O. Gunnarsson, *Phys. Rev. B* **40**, 7391 (1989).
2. U. Löw, V. J. Emery, K. Fabricius, S. A. Kivelson, *Phys. Rev. Lett.* **72**, 1918 (1994).
3. S. H. Pan *et al.*, *Nature* **413**, 282 (2001).
4. C. Howald, P. Fournier, A. Kapitulnik, *Phys. Rev. B* **64**, R100504 (2001).
5. J. E. Hoffman *et al.*, *Science* **295**, 466 (2002).
6. J. M. Tranquada, *J. Phys. Chem. Solids* **59**, 2150 (1998).
7. S. E. Ealick, *Curr. Opin. Chem. Biol.* **4**, 495 (2000).
8. M. Blume, *J. Appl. Phys.* **57**, 3615 (1985).
9. The system consists of a six-degree-of-freedom sample stage, a two-axis detector arm, a channeltron detector stage with a multilayer for fluorescence rejection, a He flow cryostat, and a 5 T magnet, operating at a base pressure of 2×10^{-10} mbar. Actuation is done with vacuum stepper motors. It resides on the X1B undulator line at the National Synchrotron Light Source.
10. I. Bozovic, *IEEE Trans. Appl. Supercond.* **11**, 2686 (2001).
11. Films of oxygen-doped $La_2CuO_{4+\delta}$ with (001) orientation were grown under tensile strain on $SrTiO_3$ by molecular beam epitaxy. Electron diffraction, atomic

force microscopy, and x-ray diffraction showed them to be atomically smooth over an area of 1 μm^2. The films were made superconducting by postannealing in ozone at 150 to 200°C for 10 to 30 min and quenching rapidly to room temperature to trap oxygen.
12. C. T. Chen *et al.*, *Phys. Rev. Lett.* **66**, 104 (1991).
13. C. T. Chen *et al.*, *Phys. Rev. Lett.* **68**, 2543 (1992).
14. F. C. Zhang, T. M. Rice, *Phys. Rev. B* **37**, R3759 (1988).
15. H. Eskes, M. B. J. Meinders, G. A. Sawatzky, *Phys. Rev. Lett.* **67**, 1035 (1991).
16. J. D. Jackson, *Classical Electrodynamics* (Wiley, New York, ed. 3, 1999).
17. Here $k = 2\pi/\lambda$, where λ is the x-ray wavelength and $n(\omega)$ is the refractive index.
18. We gratefully acknowledge the assistance of S. Hulbert, G. Nintzel, C.-C. Kao, and D. L. Feng and discussions with L. H. Tjeng, I. Elfimov, J. M. Tranquada, and J. C. Davis. Supported by an NSF IRFAP postdoctoral fellowship (INT0002581) and by the NWO (Dutch Science Foundation) via the Spinoza program. Work at the National Synchrotron Light Source is supported by the U.S. Department of Energy under contract no. DE-AC02-98CH109886.

14 February 2002; accepted 28 May 2002

Sliding Density Wave in $Sr_{14}Cu_{24}O_{41}$ Ladder Compounds

G. Blumberg,[1]* P. Littlewood,[1,2] A. Gozar,[1] B. S. Dennis,[1] N. Motoyama,[3] H. Eisaki,[4] S. Uchida[3]

We used transport and Raman scattering measurements to identify the insulating state of self-doped spin ½ two-leg ladders of $Sr_{14}Cu_{24}O_{41}$ as a weakly pinned, sliding density wave with nonlinear conductivity and a giant dielectric response that persists to remarkably high temperatures.

Investigation of the charge and spin dynamics of spin ½ low-dimensional transition metal oxide materials is attracting attention because of the critical nature of their ground state and the relevance to the phase diagram of high-temperature superconducting cuprates (*1, 2*). The competition between insulating states at low hole concentrations and superconductive pairing at higher hole densities has emerged as a key feature of the high-T_c (critical temperature) problem, but the character of the insulating states has remained elusive. Electronically one-dimensional (1D) materials are susceptible to a drastic change of their ground state to an insulator with spontaneous broken symmetry. For example, Peierls ordered states in which the links connecting nearest neighbor sites acquire modulated values for their charge and/or spin densities as well as for the exchange coupling constants are associated with broken translational symmetries and have been extensively discussed in the literature (*3*). In the charge-ordered state, collective excitations—such as those seen previously in sliding charge- and spin-density wave (C/SDW) compounds—should dominate the low-energy dynamics.

$Sr_{14}Cu_{24}O_{41}$ is an experimental realization of a two-leg ladder structure (Fig. 1). The planes of the weakly coupled Cu_2O_3 ladders are stacked along the crystallographic *b* axis alternating with 1D CuO_2 edge-sharing chain sheets (*4, 5*). The Cu-Cu distances in these two subunits are incommensurate but satisfy an approximate relation $10c_{chain} \approx 7c_{ladder}$. The legs and rungs of the ladders are along the *c* and *a* axes, respectively. Because the average valence of Cu is +2.25, the compound is intrinsically doped with holes believed to reside mainly in the chain substructure; optical studies have estimated 0.07 holes per ladder Cu site (*6*).

The self-doped compound $Sr_{14}Cu_{24}O_{41}$ is an insulator with an Arrhenius temperature dependence of the dc resistivity (*7*). Microwave (*8*) and magnetic resonance (*9*) studies have suggested the possibility of a charge ordering in the ladder planes that leads to insulating behavior. For ladders with higher hole concentrations, *d*-wave–like superconductivity was predicted to win the competition with the charge-ordered state (*1, 10*). Superconductivity at 12 K was discovered in doped two-leg ladders by applying both external and chemical pressure (*11*).

Single crystals of $Sr_{14}Cu_{24}O_{41}$ were grown as described in (*6, 12*). We have studied the low-frequency charge response by ac transport and Raman scattering experiments. The temperature dependence of the *c*-axis complex dielectric function between 10 and 10^6 Hz (Fig. 2A) was measured with a capacitive technique. The dc conductivity was measured by an electrometer (Fig. 3). Raman measurements (Fig. 2B) were performed from the (010) surface of the crystal as described in (*13*). We also report strong nonlinearity in the *c*-axis conductivity as a function of electric field.

The temperature dependence of the low-frequency Raman response function (Fig. 2B)

[1]Bell Laboratories, Lucent Technologies, Murray Hill, NJ 07974, USA. [2]University of Cambridge, Cavendish Laboratory, Cambridge CB3 0HE, UK. [3]University of Tokyo, Bunkyo-ku, Tokyo 113, Japan. [4]Stanford University, Stanford, CA 94305, USA.

*To whom correspondence should be addressed. E-mail: girsh@bell-labs.com

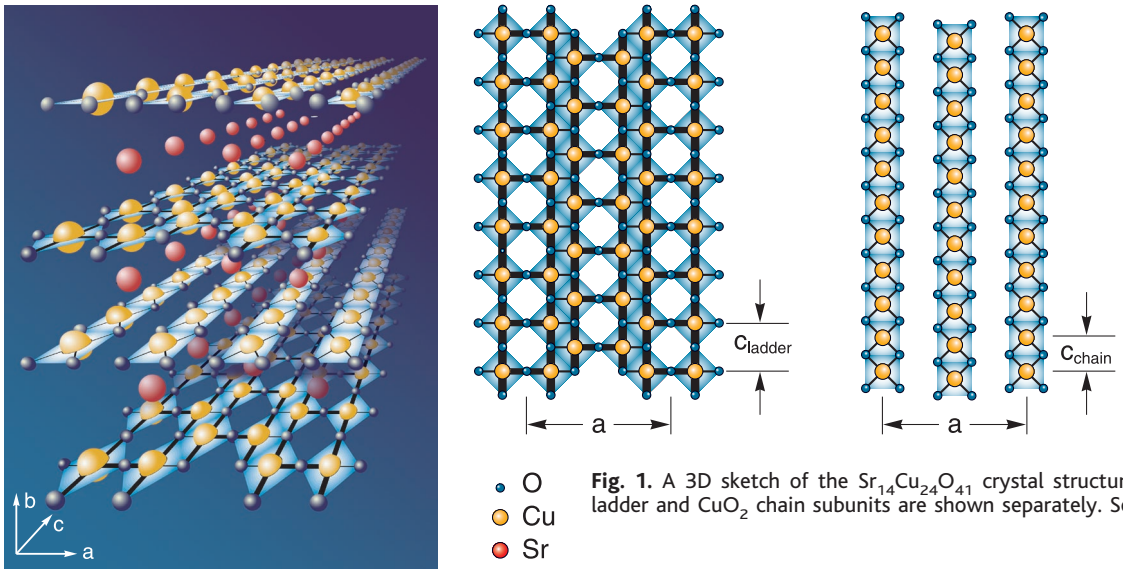

Fig. 1. A 3D sketch of the $Sr_{14}Cu_{24}O_{41}$ crystal structure. Three neighboring Cu_2O_3 ladder and CuO_2 chain subunits are shown separately. See (*4, 5*) for details.